Optimisation of Imperfection-Insensitive Continuous Tow Sheared Rocket Launch Structures

R.L. Lincoln[1], P.M. Weaver[2], A. Pirrera[3] and R.M.J. Groh[4]
Bristol Composites Institute (ACCIS), Department of Aerospace Engineering, University of Bristol, Bristol, UK

Geometric imperfection sensitivity is the largest influencing factor that limits the design of thin-walled monocoque cylinders. Current generation cylindrical architectures, such as those found in rocket launch vehicles, rely on the use of sandwich structures or blade-stiffened structures to reduce the imperfection sensitivity of the cylinder. Whilst must research has been focused on the creation of new knockdown factors that relate to the modern architectures used, this paper focuses on reducing the imperfection sensitivity of a structure from a design perspective. Variable-angle composites offer an opportunity to design the load paths of structures, thus reducing the effective area over which imperfections initiate buckling. Continuous Tow Shearing (CTS) is one such variable-angle manufacturing technique. It does not cause common in-process manufacturing defects associated with Automated Fibre Placement such as fibre wrinkling or fibre buckling. In addition, there is a fibre angle-thickness coupling that results in a local thickness build-up, which, whilst increasing the mass of the structure, enables embedded stiffeners to be created by shearing the tow. This design feature is highly desirable in cylinders, as stiffeners are known to reduce the imperfection sensitivity of the structure. It was found that the mass of a CTS cylinder is invariant of the number of embedded stringers or hoops created by the shearing process. Nonlinear finite element models with seeded imperfections are used to calculate a knockdown factor (KDF), a measure of imperfection sensitivity. It was found that there is an inverse trend between number of stringers/hoops and KDF. The best performing CTS cylinder has both a KDF 30% higher and a specific buckling load 5% higher than a QI cylinder.

I. Nomenclature

j	=	order of polynomial that defines fibre angle variation
m_0	=	S4R element size
n	=	periodicity
P_{crit}^{perf}	=	critical buckling load of a perfect cylinder
P_{crit}^{imp}	=	critical buckling load of an imperfect cylinder
t	=	nominal laminate thickness
$\bar{t}$	=	local laminate thickness
T_0	=	unsheared angle at beginning of the period

[1] PhD Researcher, Bristol Composites Institute (ACCIS), University of Bristol, UK, email: reece.lincoln@bristol.ac.uk
[2] Professor of Lightweight Structures, Bristol Composites Institute (ACCIS), University of Bristol, UK and Bernal Chair of Composite Materials and Structures, School of Engineering, University of Limerick, Castletroy, Ireland.
[3] Senior Lecturer in Composite Structures – EPSRC Research Fellow, Bristol Composites Institute (ACCIS), University of Bristol, UK.
[4] Royal Academy of Engineering Research Fellow, Bristol Composites Institute (ACCIS), University of Bristol, UK.

T_1 = sheared angle at middle of the period
θ = total angle sheared ($|T_0 - T_1|$)
ϕ = initial angle from global X-axis that defines base fibre trajectory

II. Introduction

The largest percentage (60 – 70%) of the dry mass of heavy launch vehicles is made up by the fuel and oxidizer tanks [1]. Using composite materials instead of current generation Li-Al fuel tanks is estimated to save up to 30% in mass and 25% in reoccurring manufacturing costs [1]. Research programs have aimed to use composites to capitalise on these savings but have used blade-stiffened shells or foam/honeycomb sandwich structures [2], [3]. Very few programmes have considered novel monocoque shell architectures due to the well-documented geometrical imperfection sensitivity of monocoque cylinders in compression—the design load case of heavy launch vehicles. The imperfection sensitivity is captured in the design phase of cylinders using a knockdown factor (KDF) that are applied to the theoretical critical buckling load derived from a linear eigenvalue analysis. The theoretical critical buckling pressure for a perfect isotropic cylinder is given by the formula

$$\sigma_{cr} = \frac{E\gamma}{\sqrt{3(1-\nu^2)}}\frac{t}{r}, \tag{1}$$

where the knockdown factor, γ (typically calculated using the NASA SP-8007 guideline that defines a 'lower bound' from experimental data) is given by

$$\gamma = 1 - 0.901(1 - e^{-\Gamma}), \tag{2}$$

and the exponent factor, Γ, is

$$\Gamma = \frac{1}{16}\sqrt{\frac{r}{t}} \quad \text{for} \frac{r}{t} > 1500. \tag{3}$$

The classical KDFs of the NASA SP-8007 [4] guideline are still industry-standard but have been acknowledged to be too conservative for modern materials and manufacturing tolerances. Contemporary knockdown factors have been created that are less conservative [5]–[8], but still show the imperfection sensitivity of cylindrical shells.

The imperfection sensitivity of cylinders is well-documented and explained when considering the relationship between low buckling loads and geometric imperfections in the cylinder wall as set forth in Koiter's PhD thesis [9]. Other factors do influence the low buckling loads seen in experiment (such as loading and boundary conditions [10]) but they do not consistently explain this difference in theoretical and experimental buckling loads.

The current work looks at designing monocoque cylinders that are imperfection insensitive by tailoring load paths by using a novel variable-angle tow (VAT) composite manufacturing technique, Continuous Tow Shearing (CTS) [11]. VAT composites have been shown to improve the mechanical performance of composite plates without a weight penalty [12]–[15]. It has also been shown that the imperfection sensitivity of composite cylinders can be decreased with Automated Fibre Placement (AFP) [16]. However, CTS has several benefits over AFP as a result of shearing the fibre tows instead of bending them; e.g. no in-plane bending of the tows, thus no fibre buckling or wrinkling; perfect tessellation of tows; and much smaller steering radii that leads to greater control of fibre paths. In addition to these benefits, the shearing process couples the fibre angle change to the local thickness of the tow, enabling the formation of embedded stringers and hoops perpendicular to the fibre steering direction. Fibre paths are described using the notation adapted from Gurdal [17] $\phi\langle T_0|T_1\rangle_j^n$, where ϕ is the counter-clockwise angle from the global X-axis that designates the initial direction of angle variation; T_0 is the counter-clockwise angle from ϕ that is the starting angle of the variation of fibre path; T_1 is the counter-clockwise angle from T_0 that is the angle at the middle of the 'period'; n is the number of times $\langle T_0|T_1\rangle$ occurs across the domain (herein referred to as the periodicity of the lamina); and j is the order of the polynomial that defines the change in fibre angle. Fig. 1 shows how a $90\langle 0|30\rangle_1^2$ layer is defined.

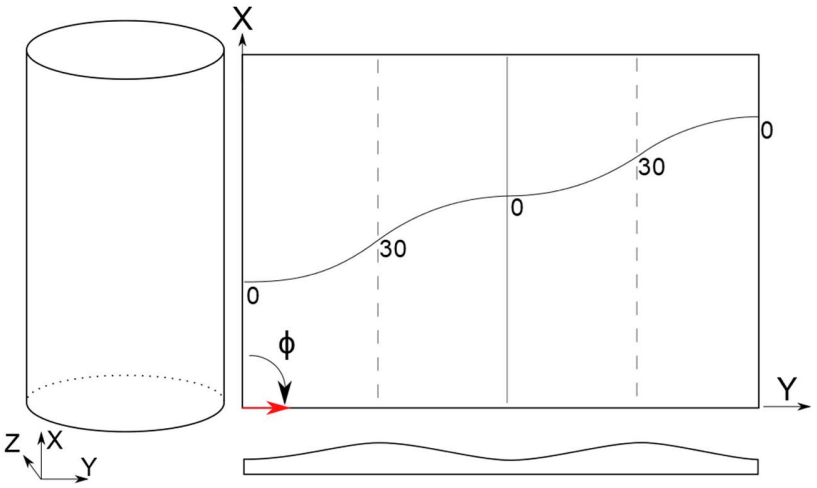

Fig. 1 A $90\langle 0|30\rangle_1^2$ lamina sheared causing two embedded-stringers to be created, shown by the cross-section.

The definition of the angle-thickness coupling is

$$t = \frac{\bar{t}}{\cos(\theta)}, \tag{4}$$

where θ is the shearing angle, which at a maximum can be 70° due to manufacturing constraints. The working hypothesis of the current study is that using the CTS technique, the imperfection sensitivity of monocoque cylinders can be decreased.

This paper aims to show preliminary data regarding CTS cylinders and to optimise a CTS cylinder with respect to the specific imperfect critical buckling load. Previous parametric studies of variables (T_0, T_1, ϕ, n) have shown that there can be an improvement in KDF and specific imperfect buckling load against a nominal QI cylinder. This paper opens the design landscape to include many more combinations of fibre-steered lamina and through a genetic algorithm an optimum layup is found.

III. Model

Multiple architectures were investigated to see the effect of tow-shearing on the imperfection sensitivity of the CTS cylinders through a parametric finite element analysis study. The definitions of the architectures are shown in Table 1.

Table 1 Designs investigated in the current study.

Design	Layup	Φ	Stiffener Type
1	$[\pm\Phi]_{2s}$	$0\langle T_0\|T_1\rangle_1^8$	Hoops
2	$[\pm\Phi]_{2s}$	$90\langle T_0\|T_1\rangle_1^{12}$	Stringers
3	$[\pm 45, \pm\Phi]_s$	$0\langle T_0\|T_1\rangle_1^8$	Hoops
4	$[\pm 45, \pm\Phi]_s$	$90\langle T_0\|T_1\rangle_1^{12}$	Stringers
5	$[\pm\Phi, 0, 90]_s$	$0\langle T_0\|T_1\rangle_1^8$	Hoops
6	$[\pm\Phi, 0, 90]_s$	$90\langle T_0\|T_1\rangle_1^{12}$	Stringers
7	$[\pm\Phi_1, \pm\Phi_2]_s$	$0\langle T_0\|T_1\rangle_1^8, 90\langle T_0\|T_1\rangle_1^{12}$	Hoops / stringers
8	$[\pm\Phi_1, \pm\Phi_2]_s$	$90\langle T_0\|T_1\rangle_1^{12}, 0\langle T_0\|T_1\rangle_1^8$	Stringers / hoops

The cylinder geometry and mechanical properties of the material system used are listed in Table 2. These parameters were used within Python-scripted Abaqus input files. The mesh size was determined after a mesh convergence study. The radius of the cylinder defined the inner surface of the cylinder wall. The total number of S4R elements is 26790 with 237 elements circumferentially and 113 elements axially. The top nodes of the model were fully fixed and the

bottom nodes were fixed apart from axial translation freedom. A displacement-controlled analysis was carried out to find the stiffness and critical buckling load of the cylinder by recording the reaction force at the top nodes.

Table 2 Material properties, cylinder geometry and element size used within the numerical model.

E_1	E_2	G_{12}	ν_{12}	R	L	t_{ply}	m_0
	GPa		-			mm	
122.2	7.332	4.9	0.31	400	1200	0.13	10.6

A Linear Buckling Analysis (LBA) and Nonlinear Buckling Analysis (NBA) are used to calculate the KDF of a given CTS cylinder. The KDF is calculated as

$$\text{KDF} = \frac{P_{crit}^{imp}}{P_{crit}^{perf}}. \tag{5}$$

The NBA used an imperfect cylinder that had pseudo-random wall imperfections seeded that were up to the magnitude of a wall thickness. The Abaqus setting NLGEOM was set to be ON to capture nonlinear geometric behaviour in the NBA.

IV. Results and discussion

Each design has increments of T_0 of 10°, ranging from 0 – 90°. Each T_0 angle has increments of T_1 of 5°, ranging from $(T_0 - 70)$ to $(T_0 + 70)$°. The axial stiffness and critical buckling mode (from a linear eigenvalue analysis) are plotted in Fig. 2 for design 6. The values are normalised against a QI cylinder $[\pm 45, 0, 90]_s$ as it is the best straight fibre laminate for axial buckling [18]. The values are also normalised against the mass of each laminate. As the fibre volume fraction is conserved when shearing, the localised thickness increases, causing an overall mass increase. The relationship between cylinder mass and total angle sheared is invariant on the periodicity, as shown in Appendix I.

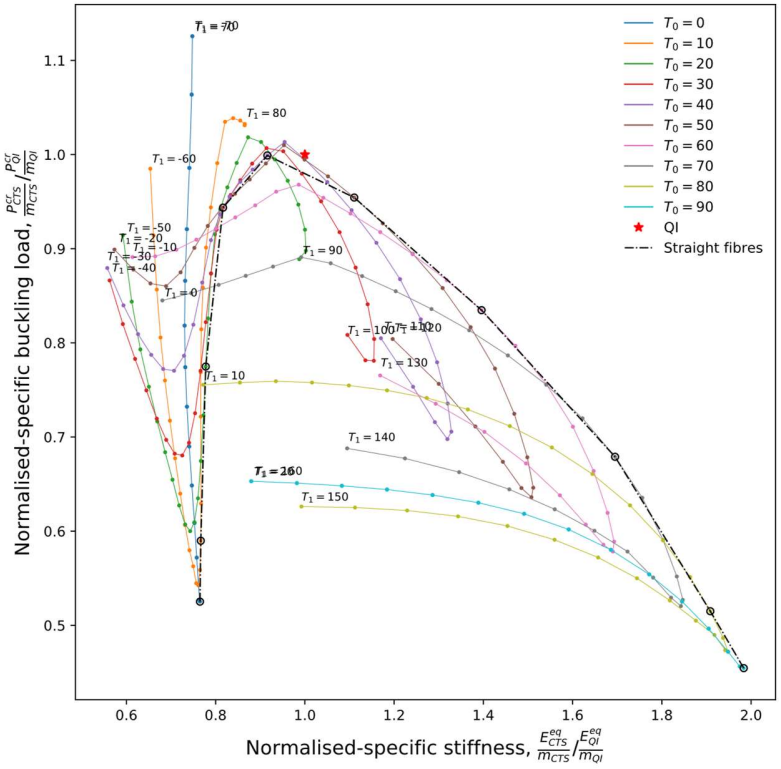

Fig. 2 Normalised axial stiffness against critical buckling load for design 6.

It can be seen from Fig. 2 that many CTS cylinder layups behave similarly to a QI cylinder on a mass-specific basis. This is a notable result as the QI cylinder has been shown to be the optimum layup for cylinder buckling [18]. Each

line on the plot designates a T_0 angle and each point on the line is an amount of shearing, given by the T_1 angle. There are several general trends that are seen when inspecting these data. Firstly, the effect of shearing on the specific buckling load and specific axial stiffness is dependent on the initial T_0 angle. Although the embedded stiffeners are still in the same direction throughout design 6, the direction of fibre at the location of the stiffening elements has a considerable impact. A T_0 angle that is initially orientated circumferentially and has a high degree of shearing ($\langle 0|70 \rangle$) results in the highest specific buckling load in design 6. One may expect that having the fibres oriented along the axis of the cylinder at the stiffeners (*e.g.* layup $\langle 20|90 \rangle$) the buckling load would be highest, but this is not the case. The circumferential fibres of the $\langle 0|70 \rangle$ laminate act to constraint the bulging buckling mode, resulting in a higher buckling load. The stiffer embedded stringers of the $\langle 20|90 \rangle$ laminate do not compensate for the lack of circumferential reinforcement, resulting in a lower buckling load.

When the initial trajectory of fibre angle is axial, the effect of shearing is a very gradual increase in specific buckling load and a dramatic decrease in specific axial stiffness. The decrease in specific axial stiffness is also nonintuitive as the shearing process creates embedded stiffeners. However, the local increase in EI contribution of the embedded stringers is minimal and the increase in mass is detrimental to the specific axial stiffness for these laminates. A second trend that is seen is that many of the laminates display 'hooking' behaviour of the specific buckling load when the shearing angle is large. Considering the family of laminates $\langle 30|T_1 \rangle$, the specific buckling load trend switches from decreasing to increasing when $T_1 = 90°$ and when $T_1 = -10°$. This behaviour happens because the increase in buckling load associated with the embedded stiffeners is now larger than the local increase in thickness and mass.

Whilst this plot contains much information, it does not consider how insensitive a given layup may be to imperfections. To understand the imperfection sensitivity of each design, an imperfect NBA is carried out. However, the current design space for all laminates considered has 2320 layups. Therefore, to narrow the number of laminates investigated, two types of inequality qualifiers on mechanical properties are used,

$$\overline{E_x} > 0.9 \text{ and } P_{crit}^{perf} > 0.9, \tag{6}$$

$$\overline{E_x} > 0.8 \text{ and } P_{crit}^{perf} > 0.8. \tag{7}$$

Eq. (6) is used for Designs 1 – 6, Eq. (7) is used for Design 7 and 8 to eliminate laminates that did not have mechanical properties similar to a QI laminate on a mass-specific basis. These 'best laminates' architectures are fed into the NBA to calculate a KDF. The KDFs for all 90 laminates are collated in Fig. 3.

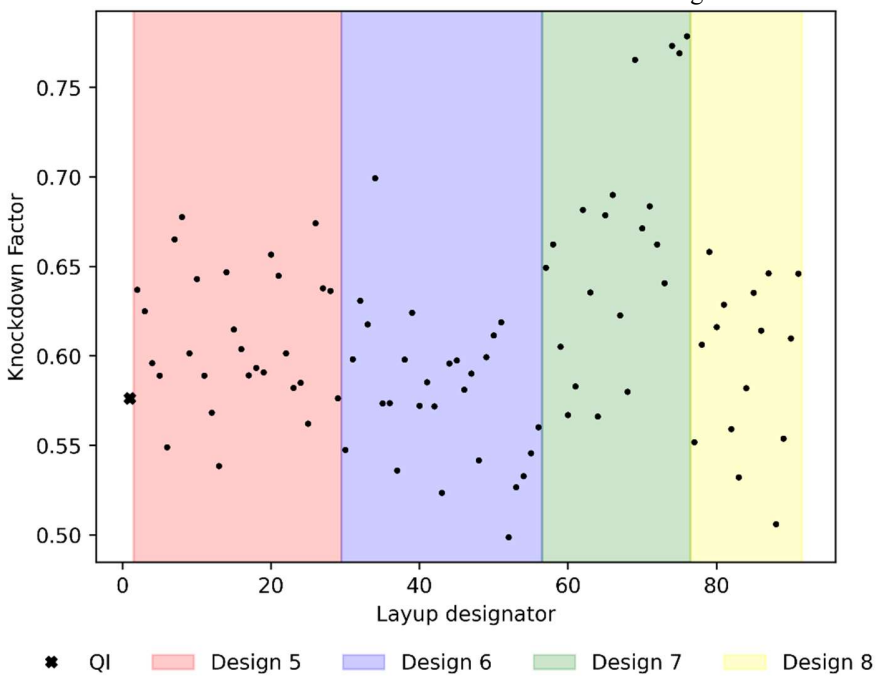

Fig. 3 Layup designator against KDF for the 'best layups' that meet the criteria in Eq. (6) and Eq. (7).

Many CTS laminates have a KDF greater than a QI laminate. These results indicate that by designing with the Continuous Tow Shearing manufacturing method, the imperfection sensitivity of a cylinder can be greatly decreased. The imperfect buckling load can also be plotted against layup designator to see the variation in imperfect buckling load, this is shown in Fig. 4.

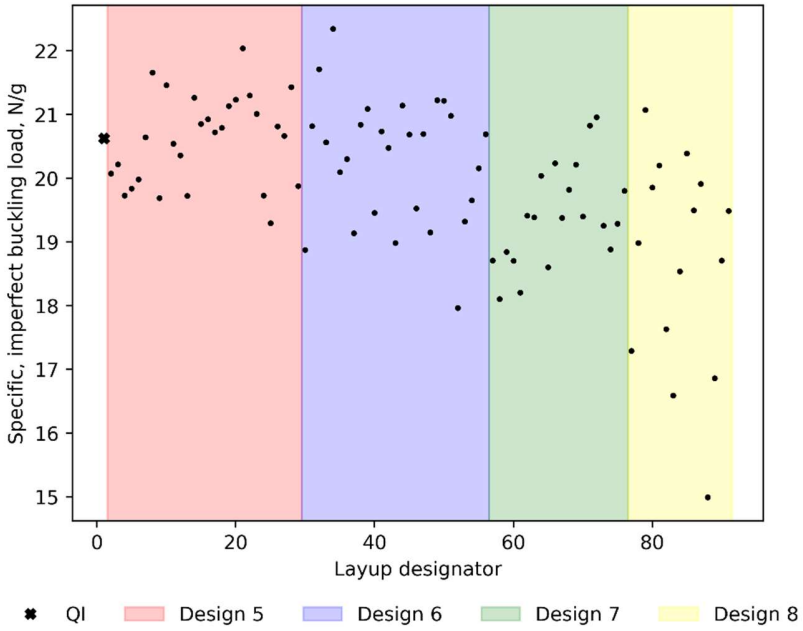

Fig. 4 Layup designator against KDF for the 'best layups' that meet the criteria in Eq. (6) and Eq. (7)

The imperfect buckling load for many laminates is comparable to an imperfect QI laminate. Design 5 and 6 have a higher average imperfect buckling load when compared to design 7 and 8. This is a consequence of the lower design inequality in Eq. (7).

V. Future work

Future work will include a genetic algorithm optimisation of CTS cylinders. The design space will be opened up to include the generic laminate $\left[\pm\phi_1\langle T_{0_1}|T_{1_1}\rangle^{n_1}, \pm\phi_2\langle T_{0_2}|T_{1_2}\rangle^{n_2}\right]_s$. The objective will be to maximise the imperfect buckling load when the seeded imperfection is a combination of the first twenty eigenmodes of a QI cylinder.

Acknowledgments

R.L. Lincoln acknowledges the support of the EPSRC [Grant No. EP/L016028/1]. P.M. Weaver acknowledges the support of the Royal Society Wolfson Merit award and the Science Foundation Ireland for the award of a Research Professor grant [Varicomp: 15/RP/2773]. A. Pirrera acknowledges the support of the EPSRC [Grant No. EP/M013170/1]. R.M.J. Groh acknowledges the support of the Royal Academy of Engineering under the Research Fellowship scheme [Grant No. RF/201718/17178].

References

[1] H. Zheng, X. Zeng, J. Zhang, and H. Sun, "The Application of Carbon Fiber Composites in Cryotank," in *Solidification*, A. E. Ares, Ed. IntechOpen, 2018, pp. 111–128.

[2] National Aeronautics and Space Administration, "Composite Cryotank Technologies & Demonstration," 2013.

[3] National Aeronautics and Space Administration, "Shell buckling knockdown factors project," 2007.

[4] National Aeronautics and Space Administration, "Space Vehicle Design: Buckling Thin-Walled Circular (SP-8007)," 1968.

[5] M. W. Hilburger, "On the development of shell buckling knockdown factors for stiffened metallic launch vehicle cylinders," in *AIAA/ASCE/AHS/ASC Structures, Structural Dynamics, and Materials Conference*, 2018, pp. 1–17.

[6] J. G. A. Croll, "Towards Simple Estimates of Shell Buckling Loads.," *Der Stahlbau*, vol. 9, no. 9, pp. 283–285, 1975.
[7] H. N. R. Wagner, E. M. Sosa, T. Ludwig, J. G. A. Croll, and C. Hühne, "Robust design of imperfection sensitive thin-walled shells under axial compression, bending or external pressure," *Int. J. Mech. Sci.*, vol. 156, no. June 2019, pp. 205–220, 2019.
[8] P. Hao *et al.*, "Worst Multiple Perturbation Load Approach of stiffened shells with and without cutouts for improved knockdown factors," *Thin-Walled Struct.*, vol. 82, pp. 321–330, 2014.
[9] W. T. Koiter, "Over de stabiliteit van het elastisch evenwicht," TU Delft, 1945.
[10] N. J. Hoff and T. C. Soong, "Buckling of circular cylindrical shells in axial compression," *Int. J. Mech. Sci.*, vol. 7, no. 7, pp. 489–520, 1965.
[11] B. C. Kim, K. Potter, and P. M. Weaver, "Continuous tow shearing for manufacturing variable angle tow composites," *Compos. Part A Appl. Sci. Manuf.*, vol. 43, no. 8, pp. 1347–1356, 2012.
[12] Z. Gurdal and R. Olmedo, "In-plane response of laminates with spatially varying fiber orientations - Variable stiffness concept," *AIAA J.*, vol. 31, no. 4, pp. 751–758, 1993.
[13] G. Raju, Z. Wu, B. C. Kim, and P. M. Weaver, "Prebuckling and buckling analysis of variable angle tow plates with general boundary conditions," *Compos. Struct.*, vol. 94, no. 9, pp. 2961–2970, 2012.
[14] Z. Wu, P. M. Weaver, and G. Raju, "Postbuckling optimisation of variable angle tow composite plates," *Compos. Struct.*, vol. 103, pp. 34–42, 2013.
[15] Z. Wu, P. M. Weaver, G. Raju, and B. Chul Kim, "Buckling analysis and optimisation of variable angle tow composite plates," *Thin-Walled Struct.*, 2012.
[16] S. C. White and P. M. Weaver, "Towards imperfection insensitive buckling response of shell structures-shells with plate-like post-buckled responses," *Aeronaut. J.*, vol. 120, no. 1224, pp. 233–253, Feb. 2016.
[17] C. S. Lopes, Z. Gürdal, and P. P. Camanho, "Variable-stiffness composite panels: Buckling and first-ply failure improvements over straight-fibre laminates," *Comput. Struct.*, vol. 86, no. 9, pp. 897–907, 2008.
[18] J. Onoda, "Optimal laminate configurations of cylindrical shells for axial buckling," *AIAA J.*, vol. 23, no. 7, pp. 1093–1098, 1985.

Appendix I

The mass of any cylinder is given by

$$m = \rho \int_0^V dV, \tag{A1}$$

where ρ is the density of the material, V is the total volume of the cylinder and dV is small volume element. This can be expanded to the integral

$$m = \rho \int_0^L \int_0^{t^*} \int_0^{2\pi r} ds\, dt\, dl\,, \tag{A2}$$

where L is the total length of the cylinder, t^* is the thickness function and $2\pi r$ is the circumference of the cylinder, ds is a small circumferential element, dt is a small thickness element and dl is a small axial element. Taking a circumferential shearing direction ($\phi = 90°$), the thickness is a function of the s-ordinate. Therefore, the first two integrals can be solved to the limits so that

$$m = \rho L \int_0^{2\pi r} t^*(s)\, ds. \tag{A3}$$

To solve $t^*(s)$, s must be found as a function of the shearing angle, θ. The relationship between t, s, and θ, is found in the expression

$$t^*(s) = \bar{t} \sec\theta\,, \text{where } \theta = \theta(s), \tag{A4}$$

so that the j-th order polynomial that defines the variation in fibre angle is

$$\theta = a s^j. \tag{A5}$$

This expression can be solved with boundary conditions [$\theta = \theta_{\max}$ at $s = \frac{2\pi r}{2n} = \frac{\pi r}{n}$] to give

$$\theta = \theta_{max} \left(\frac{n}{\pi r}\right)^j s^j. \tag{A6}$$

Thus, the expression between $s = \left[0, \frac{\pi r}{n}\right]$ is

$$t^*(s) = \bar{t}\sec\left(\theta_{max}\left(\frac{n}{\pi r}\right)^j s^j\right), \tag{A7}$$

to allow for a substitution of the original integral

$$\int_0^{2\pi r} t^*(s)\, ds = 2n\int_0^{\frac{\pi r}{n}} \bar{t}\sec\left(\theta_{max}\left(\frac{n}{\pi r}\right)^j s^j\right)\, ds. \tag{A8}$$

However, a substitution of

$$u = \sqrt[j]{\theta_m}\left(\frac{n}{\pi r}\right)s, \tag{A9}$$

to the limits of the integral gives the solution to the entire mass integral to be

$$m = \frac{2\pi r\bar{t}L\rho}{\sqrt[j]{\theta_{max}}}\int_0^{\sqrt[j]{\theta_{max}}} \sec(u^j)\ du. \tag{A10}$$

The above expression shows that the mass of cylinder is invariant to n, the periodicity.